The Effect of Imperfect Raman Pulses on the Atomic Interference Signal

M.M. Zhao[a,b], Y.J. Tan[b,*] and C.G. Shao[b]

[a] *School of Electronic and Information Engineering, Hubei University of Science and Technology, Xianning Avenue 88, Xianning 437100, China*
[b] *MOE Key Laboratory of Fundamental Physical Quantities Measurement & Hubei Key Laboratory of Gravitation and Quantum Physics, PGMF and School of Physics, Huazhong University of Science and Technology, Wuhan 430074, P.R. China*

Received: 02.05.2022 & Accepted: 13.07.2022

Doi: 10.12693/APhysPolA.142.291 *e-mail: yjtan@hust.edu.cn

Imperfect Raman pulses can lead to the formation of multiple interfering paths and affect the output of an atom interferometer in high-precision measurement. We study the effect of the imperfect Raman pulses on the interferometric fringe contrast and the phase shift in the three-pulse atom interferometer by using the evolution operator method. Analytical expressions expanded to the second-order fluctuation of imperfect pulses are derived, in which the effect of coupling the imperfect pulses with laser detuning and pulse duration is also considered. The result indicates that the second-order fluctuation of imperfect pulses is dominant, however, it can be nearly ignored in the current requirements of atomic experiments. Even so, theoretical analysis is very necessary as it may be helpful in proposing some schemes to improve the interference efficiency for future high-precision measurements with atomic interferometry.

topics: atom interferometry, imperfect Raman pulse, fringe contrast, evolution operator

1. Introduction

Atom interferometers have broad application prospects with the development of laser cooling and atom trapping technology. Due to the high stability and accuracy of the atom interferometer, it can be used to measure the gravitational acceleration [1–5], the gravity gradient [6–8], the Earth's rotation [9–14] and the Newton gravitational constant [15, 16]. Atom interferometers are also applied to test the equivalence principle [17–19] and the dark energy theories [20]. In addition, gravitational wave detections with the atom interferometer are also proposed and studied [21–25]. At present, LNE-SYRTE [14] has achieved the best rotational sensitivity 3×10^{-8} rad/(s $\sqrt{\text{Hz}}$) in rotation measurement. The HUST team achieved a short-term sensitivity of 4.2 μGal/$\sqrt{\text{Hz}}$ [5] in the gravitational acceleration measurement. In order to obtain high-precision experiment, the associated systematic errors should be carefully evaluated in the above measurements.

Raman pulses interact with atoms to split, reflect and combine atomic wave packets. The detection probability of atoms in a certain state [26] can be expressed as $P = \langle\psi(t)|\psi(t)\rangle = \frac{1}{2}(1 + C\cos(\Delta\phi))$, where $\psi(t)$ is the atomic final wave function, C is the interference fringe contrast, and $\Delta\phi$ is the differential phase shift between the two paths of the atom interferometer. There are many error sources that affect the atomic interference signal in the atomic interference experiment. Most of the errors have been studied extensively, such as the gravity gradient effect [27], the AC-Stark effect [28, 29], the second-order Zeeman effect [30, 31], the wave-front distortion effect [32], and the coupling effects of the Raman-pulse duration and gravitational field [33] or magnetic field [34]. It can be seen that with the rapid development of the atom interferometer, more and more minor systematic effects need to be taken into account. In this paper, we focus on imperfect Raman pulses that can lead to the formation of multiple quantum paths and further affect the interference signal [12, 35, 36]. Generally speaking, there are many factors that can cause the imperfect Raman pulse effect, such as fluctuations of the laser power and frequency, variations in the density of atoms interacting with laser fields [37], residual laser lines [38] and so on. We focus on the theoretical analysis of the imperfect Raman pulses due to laser fluctuation in the atomic interferometer system. In the previous work [39], we applied the evolution operator method [40, 41] to analyze the influence of the gravitational field and the Earth's rotation on the atomic interference process, in which the Raman pulses are assumed to be perfect. Here, we will use the same method to further calculate the influence of imperfect Raman pulses on the interference signal for the three-pulse atom interferometer.

2. Multiple interference paths caused by the imperfect Raman pulses

Let us assume that there are only two non-degenerate energy levels in the atomic system and there are no interactions between atoms. The internal ground state and the internal excited state of atoms can be represented by $|g\rangle$ and $|e\rangle$, respectively, in a three-pulse atom interferometer, as shown in Fig. 1.

In a perfect case, the three-pulse sequence (θ_1–θ_2–θ_3) is ($\pi/2$–π–$\pi/2$), and the interference path formed after the interaction between the atoms and the pulses is only the main path I. We assume that the atoms are in the $|g\rangle$ state with full probability at the initial time. After the first pulse is applied, half of the atoms are in the $|g\rangle$ state, and half are in the $|e\rangle$ state. After the second pulse is applied, the internal states of the atoms are reversed, and the atoms that were originally in the $|g\rangle$ (or $|e\rangle$) state jump to the $|e\rangle$ (or $|g\rangle$) state. After applying the third pulse, half the atoms in the $|g\rangle$ (or $|e\rangle$) state change to the $|e\rangle$ (or $|g\rangle$) state and the other half is still in the $|g\rangle$ (or $|e\rangle$) state — then the interference path is combined. Therefore, the atoms in the final state come from both the upper and lower paths. Finally, the transition probability of atoms in the $|g\rangle$ or $|e\rangle$ state can be obtained. Since the upper and lower paths are different, the information of the background field is reflected in the interferometric phase shift, and the target physical quantities can be obtained by detecting the atomic probability in a certain internal state.

If the pulses are not perfect, multiple paths are formed. The imperfect pulse areas are modified as $\theta_1 = \frac{\pi}{2} + \delta\theta_1$, $\theta_2 = \pi + \delta\theta_2$, $\theta_3 = \frac{\pi}{2} + \delta\theta_3$. The interference path I (purple, solid line) is formed by all three pulses (θ_1–θ_2–θ_3), the path II is built (green, densely dotted line) by the first and second pulses (θ_1–θ_2), the interference path III (yellow, densely dashed line) is built by the second and third pulses (θ_2–θ_3), and the interference path IV (red, dash–dotted line) is formed by the first and third pulses (θ_1–θ_3). Considering that the value of $\delta\theta_i$ ($i = 1, 2, 3$) is relatively small, the I-path is the main interference path. Since all of the four-path information is detected in the actual experiment, the detection of the interference signal in the main path will be affected. In order to more accurately measure the target physical quantity, the corresponding theoretical analysis must be developed and the multi-path effect must be well-estimated.

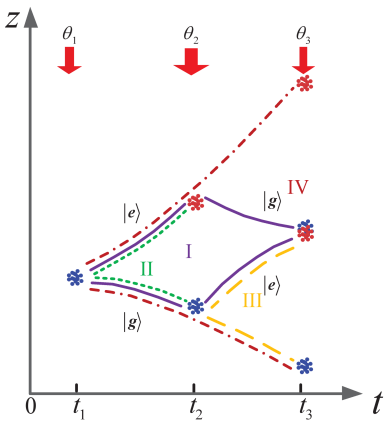

Fig. 1. Schematic diagram of multiple paths of the atom interferometry.

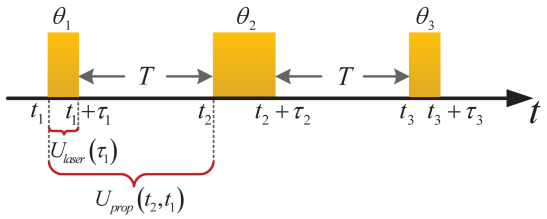

Fig. 2. Timing diagram for three-Raman-pulse sequence ($\theta_1 - \theta_2 - \theta_3$).

3. Analysis of the imperfect Raman pulses effect on the interference signal

Consider a three-pulse atom interferometer in a uniform gravitational field. The evolution operator method will be used to calculate the interfering fringe contrast and phase shift with the imperfect pulses. In this section, we first introduce the evolution operator method and then present how to model an atom interferometer with an imperfect pulse sequence.

3.1. Brief introduction of the evolution operator method

Consider an atom interferometer with a three-pulse sequence (θ_1–θ_2–θ_3). As shown in Fig. 2, the Raman pulses start at t_1, t_2, t_3, the three-pulse durations are τ_1, τ_2, τ_3, respectively, and the time interval between two consecutive pulses is T. These parameters satisfy the following relationships: $t_1 = 0$, $t_2 = T + \tau_1$, $t_3 = 2T + \tau_1 + \tau_2$, $\tau_1 = \frac{1}{2}\tau_2 = \tau_3 = \tau$. We assume that the atomic initial wave function is $|\psi(t_1)\rangle$. The time evolution operator can be expressed as $U(t_2, t_1)$ for the time from t_1 to t_2, and the wave function at t_2 can be written as

$$|\psi(t_2)\rangle = U(t_2, t_1)\,|\psi(t_1)\rangle\,. \tag{1}$$

The time evolution operator can be decomposed into the free evolution operator $U_{\text{prop}}(t_2, t_1)$ and the atom–laser interacting evolution operator $U_{\text{laser}}(\tau_1)$ using a mathematical tool. It is defined as

$$U(t_2, t_1) \equiv U_{\text{prop}}(t_2, t_1) U_{\text{laser}}(\tau_1). \tag{2}$$

In the Schrödinger picture for a two-level atom, the total Hamiltonian of the system can be expressed as

$$\hat{H}(t) = \hbar\omega_g\,|g\rangle\,\langle g| + \hbar\omega_e\,|e\rangle\,\langle e| + \frac{\hat{p}^2}{2m} + V(\boldsymbol{x}) - \boldsymbol{d}\cdot\boldsymbol{E}(t). \tag{3}$$

Here, $\hbar\omega_g$ and $\hbar\omega_e$ represent the atomic internal energy levels of ground states and excited states, respectively, m and $\hat{p}$ represent the atomic mass and the momentum operator, respectively, while $V(\boldsymbol{x})$ represents the external potential energy of the atom, which can be expressed as

$$V(x) = -m\,\boldsymbol{a}\cdot\boldsymbol{x} \tag{4}$$

with $\boldsymbol{a}$ being the atomic acceleration. The last term in (3) is the Hamiltonian of the interaction between the atoms and the light field under the dipole approximation. It can be expressed as

$$-\boldsymbol{d}\cdot\boldsymbol{E}(t) = \hbar\Omega\cos\left(\omega_L t - \boldsymbol{k}\cdot\boldsymbol{x} + \phi_0\right)\begin{pmatrix} 0 & 1 \\ 1 & 0 \end{pmatrix}. \tag{5}$$

Here, $\boldsymbol{d}$ is the electric dipole moment of a two-level atom, the effective Raman laser field can be expressed as

$$\boldsymbol{E}(t) = \boldsymbol{E}_0\cos\left(\omega_L t - \boldsymbol{k}\cdot\boldsymbol{x} + \phi_0\right), \tag{6}$$

and the Rabi frequency is

$$\Omega = -\boldsymbol{d}\cdot\boldsymbol{E}_0/\hbar \tag{7}$$

with $\boldsymbol{E}_0$, ω_L, $\boldsymbol{k}$, and ϕ_0 being the amplitude, frequency, the wave vector, and the initial phase of the laser field, respectively. According to [40, 41], the atomic free evolution matrix is derived as

$$U_{\text{prop}}(t) = \begin{bmatrix} \mathrm{e}^{-\mathrm{i}\left(\omega_e + \frac{\hat{p}^2}{2m\hbar} - m\boldsymbol{a}\cdot\boldsymbol{x}\right)t} & 0 \\ 0 & \mathrm{e}^{-\mathrm{i}\left(\omega_g + \frac{\hat{p}^2}{2m\hbar} - m\boldsymbol{a}\cdot\boldsymbol{x}\right)t} \end{bmatrix} \tag{8}$$

and the atom–laser interacting evolution matrix is obtained as

$$U_{\text{laser}}^{\theta_i}(t) = \begin{bmatrix} \mathrm{e}^{-\mathrm{i}\,\delta_i\tau_i/2} & 0 \\ 0 & \mathrm{e}^{\mathrm{i}\,\delta_i\tau_i/2} \end{bmatrix} \times \begin{bmatrix} \cos\left(\frac{\theta_i}{2}\right) + \frac{\mathrm{i}\,\delta_i\tau_i}{2}\frac{\sin(\theta_i/2)}{\theta_i/2} & -\mathrm{e}^{\mathrm{i}\,(\boldsymbol{k}\cdot\boldsymbol{x}-\phi_i)}\left(\mathrm{i}\sin\left(\frac{\theta_i}{2}\right) - \frac{(\alpha+\boldsymbol{a}\cdot\boldsymbol{k})\tau_i^2\left(\cos\left(\frac{\theta_i}{2}\right) - \frac{\sin(\theta_i/2)}{\theta_i/2}\right)}{2\theta_i}\right) \\ -\mathrm{e}^{-\mathrm{i}\,(\boldsymbol{k}\cdot\boldsymbol{x}-\phi_i)}\left(\mathrm{i}\sin(\frac{\theta_i}{2}) + \frac{(\alpha+\boldsymbol{a}\cdot\boldsymbol{k})\tau_i^2\left(\cos\left(\frac{\theta_i}{2}\right) - \frac{\sin(\theta_i/2)}{\theta_i/2}\right)}{2\theta_i}\right) & \cos\left(\frac{\theta_i}{2}\right) - \frac{\mathrm{i}\,\delta_i\tau_i}{2}\frac{\sin(\theta_i/2)}{\theta_i/2} \end{bmatrix}. \tag{9}$$

Here, $\theta_i = \omega\,\tau_i$ $(i = 1, 2, 3)$ represents i-th Raman pulse area ($\theta_1 = \theta_3 = \frac{\pi}{2}$, $\theta_2 = \pi$ for the perfect pulses), and the Rabi frequency operator is $\hat{\omega} = \sqrt{\Omega^2 + \left(\omega_L(t) - \omega_{eg} - \frac{\boldsymbol{k}\cdot\boldsymbol{p}}{m}\right)^2}$, where ω_{eg} is the frequency difference between two energy levels of the atom, $\frac{\boldsymbol{k}\cdot\boldsymbol{p}}{m}$ is the Doppler operator. The laser frequency detuning is defined as $\delta_i = \omega_L - \omega_{eg} - \frac{\boldsymbol{k}\cdot\boldsymbol{p}}{m} - (\alpha + \boldsymbol{k}\cdot\boldsymbol{a})\,t$, where α is the linear sweep slope of the light frequency and the recoil frequency shift is ignored here. One has also $\phi_i = \phi_{i,0} + \int_0^{t_i}\mathrm{d}t\,(\omega_L - \alpha\,t_i)$, for $i = 1, 2, 3$, with $\phi_{i,0}$ being the initial phase of i-th laser pulse. The atomic final wave function can be calculated by the evolution operator for the three-pulse atom interferometer as

$$\left|\psi\left(t_3+\tau_3\right)\right\rangle = U_{\text{laser}}^{\theta_3}(\tau_3)U_{\text{prop}}(t_3,t_2)U_{\text{laser}}^{\theta_2}(\tau_2) \times U_{\text{prop}}(t_2,t_1)U_{\text{laser}}^{\theta_1}(\tau_1)\left|\psi(t_1)\right\rangle. \tag{10}$$

The probability of an atom being in a certain internal state can be calculated from the atomic final wave function, and then the interferometric fringe contrast and phase shift can be obtained.

3.2. Calculating the effect of imperfect pulses in an atom interferometer

In this section the probability of finding an atom in an excited state in the uniform gravitational field $\boldsymbol{a} = \boldsymbol{g}$ is calculated, and further the effect of imperfect Raman pulses on the atom interference phase and contrast is calculated. The three imperfect pulses are denoted as $\theta_1 = \frac{\pi}{2} + \delta\theta_1$, $\theta_2 = \pi + \delta\theta_2$, $\theta_3 = \frac{\pi}{2} + \delta\theta_3$. Substituting them into (9), we expand each matrix element to the second order term of $\delta\theta_i$ $(i = 1, 2, 3)$. Then, the atom–laser interacting evolution matrix for the first or third imperfect pulse $(i = 1, 3)$ can be written as

$$U_{\text{laser}}^{\theta_i}(\tau_i) = \frac{1}{\sqrt{2}}\begin{bmatrix} M_{11}(\theta_i,\tau_i,\delta_i)\,\mathrm{e}^{-\mathrm{i}\,\delta_i\tau_i/2} & M_{12}(\theta_i,\tau_i,\delta_i)\,\mathrm{e}^{-\mathrm{i}\,\delta_i\tau_i/2}\,\mathrm{e}^{\mathrm{i}\,(\boldsymbol{k}\cdot\boldsymbol{x}-\phi_i)} \\ M_{21}(\theta_i,\tau_i,\delta_i)\,\mathrm{e}^{\mathrm{i}\,\delta_i\tau_i/2}\,\mathrm{e}^{-\mathrm{i}\,(\boldsymbol{k}\cdot\boldsymbol{x}-\phi_i)} & M_{22}(\theta_i,\tau_i,\delta_i)\,\mathrm{e}^{\mathrm{i}\,\delta_i\tau_i/2} \end{bmatrix} \tag{11}$$

with

$$M_{11}(\theta_i,\tau_i,\delta_i)=\mathrm{e}^{\frac{2\,\mathrm{i}\,\delta_i\tau_i}{\pi}}-\frac{1}{2}\delta\theta_i\,\mathrm{e}^{-\frac{2\,\mathrm{i}\,(\pi-4)\delta_i\tau_i}{\pi^2}}-\frac{1}{8}{\delta\theta_i}^2\,\mathrm{e}^{\frac{2\,\mathrm{i}\,(\pi^2+8\pi-32)\delta_i\tau_i}{\pi^3}},$$

$$M_{12}(\theta_i,\tau_i,\delta_i)=-\mathrm{i}\,\mathrm{e}^{\frac{\mathrm{i}\,(\pi-4)(\alpha+\boldsymbol{g}\cdot\boldsymbol{k}){\tau_i}^2}{\pi^2}}-\frac{\mathrm{i}}{2}\delta\theta_i\,\mathrm{e}^{-\frac{\mathrm{i}\,(\pi^2+8\pi-32)(\alpha+\boldsymbol{g}\cdot\boldsymbol{k}){\tau_i}^2}{\pi^3}}+\frac{\mathrm{i}}{8}\delta\theta_i^2\,\mathrm{e}^{\frac{\mathrm{i}\,(\pi^3-12\pi^2-96\pi+384)(\alpha+\boldsymbol{g}\cdot\boldsymbol{k})\tau_i^2}{\pi^4}},$$

$$M_{21}(\theta_i,\tau_i,\delta_i)=-\mathrm{i}\,\mathrm{e}^{-\frac{\mathrm{i}\,(\pi-4)(\alpha+\boldsymbol{g}\cdot\boldsymbol{k})\tau_i^2}{\pi^2}}-\frac{\mathrm{i}}{2}\delta\theta_i\,\mathrm{e}^{\frac{\mathrm{i}\,(\pi^2+8\pi-32)(\alpha+\boldsymbol{g}\cdot\boldsymbol{k})\tau_i^2}{\pi^3}}+\frac{\mathrm{i}}{8}\delta\theta_i^2\,\mathrm{e}^{-\frac{\mathrm{i}\,(\pi^3-12\pi^2-96\pi+384)(\alpha+\boldsymbol{g}\cdot\boldsymbol{k})\tau_i^2}{\pi^4}},$$

$$M_{22}(\theta_i,\tau_i,\delta_i)=\mathrm{e}^{-\frac{2\,\mathrm{i}\,\delta_i\tau_i}{\pi}}-\frac{1}{2}\delta\theta_i\,\mathrm{e}^{\frac{2\,\mathrm{i}\,(\pi-4)\delta_i\tau_i}{\pi^2}}-\frac{1}{8}{\delta\theta_i}^2\,\mathrm{e}^{-\frac{2\,\mathrm{i}\,(\pi^2+8\pi-32)\delta_i\tau_i}{\pi^3}}. \tag{12}$$

Similarly, the atom–laser interacting evolution matrix for the second imperfect pulse can be obtained as

$$U_{\mathrm{laser}}^{\theta_2}(\tau_2)=\begin{bmatrix} M'_{11}(\theta_2,\tau_2,\delta_2)\,\mathrm{e}^{-\mathrm{i}\,\delta_2\tau_2/2} & M'_{12}(\theta_2,\tau_2,\delta_2)\,\mathrm{e}^{-\mathrm{i}\,\delta_2\tau_2/2}\,\mathrm{e}^{\mathrm{i}\,(\boldsymbol{k}\cdot\boldsymbol{x}-\phi_2)} \\ M'_{21}(\theta_2,\tau_2,\delta_2)\,\mathrm{e}^{\mathrm{i}\,\delta_2\tau_2/2}\,\mathrm{e}^{-\mathrm{i}\,(\boldsymbol{k}\cdot\boldsymbol{x}-\phi_2)} & M'_{22}(\theta_2,\tau_2,\delta_2)\,\mathrm{e}^{\mathrm{i}\,\delta_2\tau_2/2} \end{bmatrix} \tag{13}$$

with

$$M'_{11}(\theta_2,\tau_2,\delta_2)=\left(\mathrm{e}^{\frac{\mathrm{i}\,\delta_2\tau_2}{\pi}}-1\right)-\frac{1}{2}\delta\theta_2\,\mathrm{e}^{\frac{2\,\mathrm{i}\,\delta_2\tau_2}{\pi^2}}+\left(\mathrm{e}^{-\frac{\mathrm{i}\,(\pi^2-8)\delta_2\tau_2}{8\pi^3}}-1\right)\delta\theta_2^2,$$

$$M'_{12}(\theta_2,\tau_2,\delta_2)=-\mathrm{i}\,\mathrm{e}^{-\frac{\mathrm{i}\,(\alpha+\boldsymbol{g}\cdot\boldsymbol{k})\tau_2^2}{\pi^2}}-\frac{(\pi^2-8)(\alpha+\boldsymbol{g}\cdot\boldsymbol{k})}{4\pi^3}\,\delta\theta_2\tau_2^2+\frac{\mathrm{i}}{8}\mathrm{e}^{-\frac{3\,\mathrm{i}\,(\pi^2-8)(\alpha+\boldsymbol{g}\cdot\boldsymbol{k})\tau_2^2}{\pi^4}}\delta\theta_2^2,$$

$$M'_{21}(\theta_2,\tau_2,\delta_2)=-\mathrm{i}\,\mathrm{e}^{\frac{\mathrm{i}\,(\alpha+\boldsymbol{g}\cdot\boldsymbol{k})\tau_2^2}{\pi^2}}+\frac{(\pi^2-8)(\alpha+\boldsymbol{g}\cdot\boldsymbol{k})}{4\pi^3}\,\delta\theta_2\tau_2^2+\frac{\mathrm{i}}{8}\mathrm{e}^{\frac{3\,\mathrm{i}\,(\pi^2-8)(\alpha+\boldsymbol{g}\cdot\boldsymbol{k})\tau_2^2}{\pi^4}}\delta\theta_2^2,$$

$$M'_{22}(\theta_2,\tau_2,\delta_2)=\left(\mathrm{e}^{-\frac{\mathrm{i}\,\delta_2\tau_2}{\pi}}-1\right)-\frac{1}{2}\delta\theta_2\,\mathrm{e}^{-\frac{2\,\mathrm{i}\,\delta_2\tau_2}{\pi^2}}+\left(\mathrm{e}^{\frac{\mathrm{i}\,(\pi^2-8)\delta_2\tau_2}{8\pi^3}}-1\right)\delta\theta_2^2. \tag{14}$$

The atomic free evolution matrix can be obtained as

$$U_{\mathrm{prop}}(t_2,t_1)=\begin{bmatrix} \exp\left(-\mathrm{i}\int\limits_{t_1}^{t_2}\mathrm{d}t\left(\omega_e+\frac{\left|\boldsymbol{p}+\frac{\hbar\boldsymbol{k}}{2}+m\boldsymbol{g}t\right|^2}{2m\hbar}\right)\right) & 0 \\ 0 & \exp\left(-\mathrm{i}\int\limits_{t_1}^{t_2}\mathrm{d}t\left(\omega_g+\frac{\left|\boldsymbol{p}-\frac{\hbar\boldsymbol{k}}{2}+m\boldsymbol{g}t\right|^2}{2m\hbar}\right)\right) \end{bmatrix}, \tag{15}$$

$$U_{\mathrm{prop}}(t_3,t_2)=\begin{bmatrix} \exp\left(-\mathrm{i}\int\limits_{t_2}^{t_3}\mathrm{d}t\left(\omega_e+\frac{\left|\boldsymbol{p}+\frac{\hbar\boldsymbol{k}}{2}+m\boldsymbol{g}t\right|^2}{2m\hbar}\right)\right) & 0 \\ 0 & \exp\left(-\mathrm{i}\int\limits_{t_2}^{t_3}\mathrm{d}t\left(\omega_g+\frac{\left|\boldsymbol{p}-\frac{\hbar\boldsymbol{k}}{2}+m\boldsymbol{g}t\right|^2}{2m\hbar}\right)\right) \end{bmatrix}. \tag{16}$$

By applying the above time evolution operators to the atomic initial wave function in turn, the atomic final wave function can be derived by (10). Assuming that the atoms are in the ground state with full probability at the initial times $t_1=0$, the atomic initial wave function is expressed as

$$\left|\psi(t_1)\right\rangle=\begin{bmatrix}\psi_e(t_1)\\ \psi_g(t_1)\end{bmatrix}=\begin{bmatrix}0\\ \mathrm{e}^{\mathrm{i}\,(\frac{\boldsymbol{p}}{\hbar}-\frac{\boldsymbol{k}}{2})\cdot\boldsymbol{x}}\end{bmatrix}. \tag{17}$$

Based on (10), the atomic probability in the excited state can be obtained approximately as

$$\begin{aligned}P=&\frac{1}{2}\left[1+\delta\theta_1\delta\theta_3+A_1\cos\left(\phi_{1,0}-2\phi_{2,0}+\phi_{3,0}+B_1-\frac{\pi}{2}\right)\right]\\&+\frac{1}{2}A_2\cos\left(\phi_{1,0}-\phi_{2,0}-\delta_0T+B_2-\frac{\pi}{2}\right)+\frac{1}{2}A_3\cos\left(\phi_{2,0}-\phi_{3,0}-\delta_0T+B_3-\frac{\pi}{2}\right)\\&+\frac{1}{2}A_4\cos\left(\phi_{1,0}-\phi_{3,0}-2\delta_0T+B_4-\frac{\pi}{2}\right),\end{aligned} \tag{18}$$

where

$$A_1 = \sqrt{\left(\tfrac{1}{2}\delta\theta_1^2 + \tfrac{1}{4}\delta\theta_2^2 + \tfrac{1}{2}\delta\theta_3^2 - 1\right)^2 + \left[\begin{array}{l} -(\frac{4}{\pi^2}-\frac{2}{\pi})\delta_0\tau\delta\theta_1 + (\frac{8}{\pi^3}-\frac{4}{\pi^2}+\frac{1}{\pi})\delta_0\tau\delta\theta_1{}^2 \\ +(\frac{4}{\pi^2}-\frac{2}{\pi})\delta_0\tau\delta\theta_3 - (\frac{8}{\pi^3}-\frac{4}{\pi^2}+\frac{1}{\pi})\delta_0\tau\delta\theta_3{}^2 \\ -(\alpha+\boldsymbol{k}\cdot\boldsymbol{g})\left[\begin{array}{l} 1+\frac{2\tau}{T}-\frac{4\tau}{\pi T}+\frac{\tau}{\pi T}\,\delta\theta_2^2+\frac{2\tau}{\pi T}\,\delta\theta_1^2 \\ +(\frac{2}{\pi^2}-\frac{1}{\pi})\,\frac{4\tau}{T}\delta\theta_3-(\frac{2}{\pi^3}-\frac{1}{\pi^2})\frac{8\tau}{T}\,\delta\theta_3^2 \end{array}\right]T^2 \end{array}\right]^2}, \tag{19}$$

$$A_2 = \sqrt{\delta\theta_2^2\delta\theta_3^2 + \left[\tfrac{4}{\pi}\delta_0\tau\delta\theta_3 - \left(\tfrac{2}{\pi}+\tfrac{4}{\pi^2}\right)\delta_0\tau\delta\theta_2\delta\theta_3 + \tfrac{1}{2}(\alpha+\boldsymbol{k}\cdot\boldsymbol{g})\left(1+\tfrac{2\tau}{T}-\tfrac{8\tau}{T}\delta\theta_3+\tfrac{8\tau}{\pi^2 T}\delta\theta_2\delta\theta_3\right)T^2\right]^2}, \tag{20}$$

$$A_3 = \sqrt{\delta\theta_1^2\delta\theta_2^2 + \left[\tfrac{4}{\pi}\delta_0\tau\delta\theta_1 - \left(\tfrac{2}{\pi}+\tfrac{4}{\pi^2}\right)\delta_0\tau\delta\theta_1\delta\theta_2 + \tfrac{3}{2}(\alpha+\boldsymbol{k}\cdot\boldsymbol{g})\left(1+\tfrac{2\tau}{T}-\tfrac{8\tau}{3\pi T}\delta\theta_1+(\tfrac{1}{\pi^2}+\tfrac{1}{\pi})\tfrac{8\tau}{3T}\,\delta\theta_1\delta\theta_2\right)T^2\right]^2}, \tag{21}$$

$$A_4 = \sqrt{\tfrac{1}{4}\delta\theta_2^2 + \left[\tfrac{2}{\pi}\delta_0\tau\delta\theta_2 - \left(\tfrac{1}{\pi}+\tfrac{2}{\pi^2}\right)\delta_0\tau\delta\theta_2^2 - 2(\alpha+\boldsymbol{k}\cdot\boldsymbol{g})\left(1+\tfrac{4\tau}{T}+\tfrac{\tau}{\pi T}\delta\theta_2-(\tfrac{1}{2\pi}+\tfrac{1}{\pi^2})\tfrac{\tau}{T}\,\delta\theta_2^2\right)T^2\right]^2}, \tag{22}$$

$$B_1 = \arcsin\left(\frac{\frac{1}{2}\delta\theta_1^2 + \frac{1}{4}\delta\theta_2^2 + \frac{1}{2}\delta\theta_3^2 - 1}{A_1}\right), \tag{23}$$

$$B_2 = \arcsin\left(\frac{\delta\theta_2\delta\theta_3}{A_2}\right), \tag{24}$$

$$B_3 = \arcsin\left(\frac{\delta\theta_1\delta\theta_2}{A_3}\right), \tag{25}$$

$$B_4 = \arcsin\left(\frac{\delta\theta_2^2}{4A_4}\right). \tag{26}$$

Here, δ_0 is the laser detuning at the initial time $t_1 = 0$. The above equations maintain the first-order term of τ and the second-order term of $\delta\theta_i$.

3.3. Discussion

From (18), one can intuitively get the fringe contrasts A_1, A_2, A_3, A_4, respectively corresponding to the four interfering paths I, II, III, IV in Fig. 1. In an ideal case, i.e., $A_1 = 1$, $A_2 = A_3 = A_4 = 0$, only the I-path exists. In the case of (19)–(22) and (23)–(26) they demonstrate the effect of imperfect pulses on the interfering fringe contrast and phase shift, respectively. The corresponding analytical expressions expanded to the second-order fluctuation of imperfect pulses are given. They also take into account the coupling effect of the imperfect pulses with the laser detuning and pulse duration. The result indicates that the second-order fluctuation of imperfect pulses is dominant. Note that the coupling effect of gravity acceleration and imperfect pulses $\delta\theta_i$ can be ignored because the gravity-induced Doppler shift can be compensated by adjusting the linear sweep slope α to satisfy $\alpha + \boldsymbol{k}\cdot\boldsymbol{g} \approx 0$. This means that the main effect is independent of the effective wave vector. Therefore, the Doppler-insensitive interferometer is suitable to study the multi-path effect since it is not easy to distinguish the main path from other redundant paths in the Doppler-sensitive interferometer.

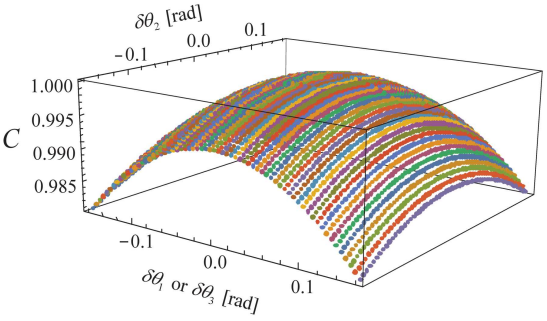

Fig. 3. Interfering fringe contrast varying with both the first (or third) and second imperfect pulses.

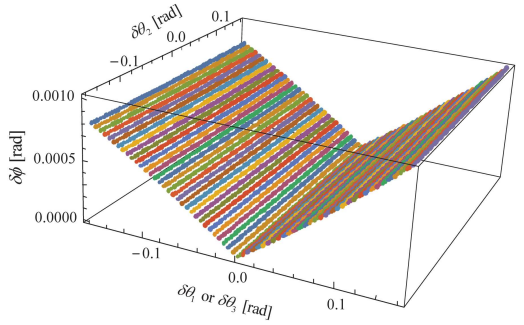

Fig. 4. Change of the phase shift with the first (or third) and second imperfect pulses.

In general, we are focusing is on the influence of imperfect Raman pulses on the main interfering path. In this case, the fringe contrast and the change of the phase shift can be written as $C = A_1$, $\delta\phi = B_1 - \pi/2$. We use the typical experimental parameters, i.e., the laser detuning $\delta_0 = 1$ kHz, the pulse duration $\tau = 24$ μs, and the Rabi frequency $\omega = 6.5 \times 10^4$ Hz. The pulse fluctuation $\delta\theta_i = \Delta\omega\,\tau$ can be estimated as -0.16–0.16 rad

with Rabi frequency fluctuation $\Delta\omega = \frac{1}{10}\omega$. We plot the interfering fringe contrast and the phase shift varying with $\delta\theta_i$ as shown in Fig. 3 and Fig. 4, respectively. As the effects of $\delta\theta_1$ and $\delta\theta_3$ are similar, only the fringe contrast and the phase shift varying with both $\delta\theta_1$ (or $\delta\theta_3$) and $\delta\theta_2$ are given. In Fig. 3, the effect of imperfect pulses on the fringe contrast is less than two percent. In Fig. 4, the effect of imperfect pulses on the phase shift is less than 1 mrad. Specially, when $\delta\theta_1 = \delta\theta_3$, the change of the phase shift is $\delta\phi = 0$ regardless of the value of $\delta\theta_2$. According to (18), the multi-path effect can be eliminated by adjusting Raman pulse-related parameters. Some methods of eliminating this effect have also been proposed, e.g., modifying the timing of the laser pulses [12] or through the stimulated Raman adiabatic technology [42, 43].

4. Conclusion

We present a theoretical analysis on the atomic interference signal due to the imperfect pulses effect in a three-pulse atom interferometer and give the corresponding analytical expressions using the evolution operator method. Based on typical parameters, we evaluate this effect on the interferometric fringe contrast and the phase shift, and find the second-order fluctuation of imperfect pulses is dominant compared to the first-order effect. This work presents a detailed calculation for the imperfect pulse effect that may give a useful theoretical reference for research to improve the interference efficiency for a higher precision atom interfering experiment.

Acknowledgments

This work is supported by the National Natural Science Foundation of China (Grant Nos. 11805074)

References

[1] A. Peters, K.Y. Chung, S. Chu, *Metrologia* **38**, 25 (2001).

[2] J. L.Gouët, T. Mehlstäubler, J. Kim, S. Merlet, A. Clairon, A. Landragin, F. Pereira Dos Santos, *Appl. Phys. B* **92**, 133 (2008).

[3] M.-K. Zhou, Z.-K. Hu, X.-C. Duan, B.-L. Sun, L.-L. Chen, Q.-Z. Zhang, J. Luo, *Phys. Rev. A* **86**, 043630 (2012).

[4] F. Sorrentino, A. Bertoldi, Q. Bodart, L. Cacciapuoti, M. de Angelis, Y.-H. Lien, M. Prevedelli, G. Rosi, G.M. Tino, *Appl. Phys. Lett.* **101**, 114106 (2012).

[5] Z.K. Hu, B.L. Sun, X.C. Duan, M.K. Zhou, L.L. Chen, S. Zhan, Q.Z. Zhang, J. Luo, *Phys. Rev. A* **88**, 043610 (2013).

[6] M. Snadden, J. McGuirk, P. Bouyer, K. Haritos, M. Kasevich, *Phys. Rev. Lett.* **81**, 971 (1998).

[7] F. Sorrentino, Q. Bodart, L. Cacciapuoti, Y.H. Lien, M. Prevedelli, G. Rosi, L. Salvi, G.M. Tino, *Phys. Rev. A* **89**, 023607 (2014).

[8] X.C. Duan, M.K. Zhou, D.K. Mao, H.B. Yao, X.B. Deng, J. Luo, Z.K. Hu, *Phys. Rev. A* **90**, 023617 (2014).

[9] T.L. Gustavson, P. Bouyer, M.A. Kasevich, *Phys. Rev. Lett.* **78**, 2046 (1997).

[10] B. Canuel, F. Leduc, D. Holleville et al., *Phys. Rev. Lett.* **97**, 010402 (2006).

[11] R. Trubko, J. Greenberg, A.D. Cronin, *Phys. Rev. Lett.* **114**, 140404 (2015).

[12] J.K. Stockton, K. Takase, M.A. Kasevich, *Phys. Rev. Lett.* **107**, 133001 (2011).

[13] I. Dutta, D. Savoie, B. Fang, B. Venon, C.L. Garrido Alzar, R. Geiger, A. Landragin, *Phys. Rev. Lett.* **116**, 183003 (2016).

[14] D. Savoie, M. Altorio, B. Fang, L. Sidorenkov, R. Geiger, A. Landragin, *Sci. Adv.* **4**, 7948 (2018).

[15] J.B. Fixler, G. Foster, J. McGuirk, M. Kasevich, *Science* **315**, 74 (2007).

[16] G. Rosi, F. Sorrentino, L. Cacciapuoti, M. Prevedelli, G. Tino, *Nature* **510**, 518 (2014).

[17] P. Asenbaum, C. Overstreet, M. Kim, J. Curti, M.A. Kasevich, *Phys. Rev. Lett.* **125**, 191101 (2020).

[18] X.C. Duan, X.B. Deng, M.K. Zhou et al., *Phys. Rev. Lett.* **117**, 023001 (2016).

[19] G. Rosi, G. D'Amico, L. Cacciapuoti, F. Sorrentino, M. Prevedelli, M. Zych, Č. Brukner, G. Tino, *Nat. Commun.* **8**, 15529 (2017).

[20] M. Jaffe, P. Haslinger, V. Xu, P. Hamilton, A. Upadhye, B. Elder, J. Khoury, H. Müller, *Nature Phys.* **13**, 13 938 (2017).

[21] Dimopoulos S, Graham PW, J.M. Hogan, M.A. Kasevich, *Phys. Rev. Lett.* **98**, 111102 (2007).

[22] Y.J. Wang, X.Y. Lu, C.G. Qin, Y.J. Tan, C.G. Shao, *Class. Quantum Grav.* **38**, 145025 (2021).

[23] N. Yu, M. Tinto, *Gen. Relativ. Gravit.* **43**, 1943 (2011).

[24] S. Dimopoulos, P.W. Graham, J.M. Hogan, M.A. Kasevich, S. Rajendran, *Phys. Rev. D* **78**, 122002 (2008).

[25] P.W. Graham, J.M. Hogan, M.A. Kasevich, S. Rajendran, *Phys. Rev. Lett.* **110**, 171102 (2013).

[26] A. Roura, W. Zeller, W.P. Schleich, *New J. Phys.* **16**, 123012 (2014).

[27] P. Wolf, P. Tourrenc, *Phys. Rev. A* **251**, 241 (1999).

[28] M.A. Kasevich, S. Chu, *Phys. Rev. Lett.* **67**, 181 (1991).

[29] A. Gauguet, B. Canuel, T. Lévèque, W. Chaibi, A. Landragin, *Phys. Rev. A* **80**, 063604 (2009).

[30] Q.Q. Hu, C. Freier, B. Leykauf, V. Schkolnik, J. Yang, M. Krutzik, A. Peters, *Phys. Rev. A* **96**, 033414 (2017).

[31] B. Wu, Z. Wang, B. Cheng, Q. Wang, A. Xu, Q. Lin, *Metrologia* **51**, 452 (2014).

[32] M.K. Zhou, Q. Luo, X.C. Duan, Z.K. Hu, *Phys. Rev. A* **93**, 043610 (2016).

[33] C.G. Shao, D.K. Mao, M.K. Zhou, Y.J. Tan, L.L. Chen, J. Luo, Z.K. Hu, *Phys. Rev. A* **92**, 053613 (2015).

[34] Y. Cheng, Y.J. Tan, M.K. Zhou, X.C. Duan, C.G. Shao, Z.K. Hu, *Chin. Phys. B* **27**, 030303 (2018).

[35] K. Takase, Ph.D. Thesis, Stanford University, 2008.

[36] S.B. Lu, Z.W. Yao, R.B. Li et al., *Opt. Commun.* **429**, 158 (2018).

[37] Q.Q. Hu, Y.K. Luo, A.A. Jia, C.H. Wei, S.H. Yan, J. Yang, *Opt. Commun.* **390**, 111 (2017).

[38] S. Templier, J. Hauden, P. Cheiney, F. Napolitano, H. Porte, P. Bouyer, B. Barrett, B. Battelier, *Phys. Rev. Applied* **16**, 044018 (2021).

[39] X. Li, C.G. Shao, Z.K. Hu, *J. Opt. Soc. Am. B* **32**, 248 (2015).

[40] K.P. Marzlin, J. Audretsch, *Phys. Rev. A* **53**, 1004 (1996).

[41] Y.-J. Tan, M.-M. Zhao, P.-P. Wang Y.-J. Wang, Y.-Y. Xu, X.-C. Duan, C.-G. Shao, Z.-K. Hu, *Metrologia* **57**, 035006 (2020).

[42] K. Kotru, J.M. Brown, D.L. Butts, J.M. Kinast, R.E. Stoner, *Phys. Rev. A* **90**, 053611 (2014).

[43] K. Kotru, D.L. Butts, J.M. Kinast, R.E. Stoner, *Phys. Rev. Lett.* **115**, 103001 (2015).